

Genome-wide DNA copy number profiling and bioinformatics analysis of ovarian cancer reveals key genes and pathways associated with distinct invasive/migratory capabilities

GuiFen Liu¹, GuanYu Ruan¹, MeiMei Huang¹, LiLi Chen¹, PengMing Sun^{1,2}

¹Laboratory of Gynaecologic Oncology, Fujian Provincial Maternity and Children's Hospital, Affiliated Hospital of Fujian Medical University, Fuzhou 350001, Fujian Province, China

²Department of Gynaecology, Fujian Provincial Maternity and Children's Hospital, Affiliated Hospital of Fujian Medical University, Fuzhou 350001, Fujian Province, China

Correspondence to: Pengming Sun; email: sunfemy@hotmail.com

Keywords: copy number variations (CNVs), protein/DNA array, ovarian cancer, invasion, metastasis

Received: June 22, 2019

Accepted: December 5, 2019

Published: January 2, 2020

Copyright: Liu et al. This is an open-access article distributed under the terms of the Creative Commons Attribution License (CC BY 3.0), which permits unrestricted use, distribution, and reproduction in any medium, provided the original author and source are credited.

ABSTRACT

Ovarian cancer (OC) metastasis presents major hurdles that must be overcome to improve patient outcomes. Recent studies have demonstrated copy number variations (CNVs) frequently contribute to alterations in oncogenic drivers. The present study used a CytoScan HD Array to analyse CNVs and loss of heterozygosity (LOH) in the entire genomes of 6 OC patients and human OC cell lines to determine the genetic target events leading to the distinct invasive/migratory capacities of OC. The results showed that LOH at Xq11.1 and Xp21.1 and gains at 8q21.13 were novel, specific CNVs. Ovarian cancer-related CNVs were then screened by bioinformatics analysis. In addition, transcription factors-target gene interactions were predicted with information from PASTAA analysis. As a result, six genes (i.e., GAB2, AKT1, EGFR, COL6A3, UGT1A1 and UGT1A8) were identified as strong candidates by integrating the above data with gene expression and clinical outcome data. In the transcriptional regulatory network, 4 known cancer-related transcription factors (TFs) interacted with 6 CNV-driven genes. The protein/DNA arrays revealed 3 of these 4 TFs as potential candidate gene-related transcription factors in OC. We then demonstrated that these six genes can serve as potential biomarkers for OC. Further studies are required to elucidate the pathogenesis of OC.

INTRODUCTION

Ovarian cancer (OC) is a deadly disease that affects women globally. The worldwide incidence of OC is currently 225,500 new diagnoses each year [1–2]. High-grade OC generally grows rapidly, metastasizes early, and has a very aggressive disease course and high rate of chemotherapy resistance [3]. Thus, metastasis and resistance represent major hurdles that must be overcome. Cancer expands clonally and originates from a single clonal state; this expansion is accompanied by genetic changes that lead to functional differences, resulting in different stages and characteristics of tumour development [4–5].

Copy number variations (CNVs) are DNA fragments ranging in size from 1 kilobase (kb) to several megabases (Mb) that arise due to duplication or deletion events. A growing number of studies have reported that CNVs are correlated with the genetic and phenotypic diversity of tumours and are frequently associated with the activation of oncogenic drivers or the deletion of tumour suppressor factors [6–9]. Previous studies using either conventional metaphase chromosome-based comparative genomic hybridization [10–11] or array-based high-resolution genomic technology to identify genome-wide CNVs in OC [12–19] have identified regions of frequently increased copy number along chromosomes 1, 3, 7, 8, 17 and 20 and reduced copy number along chromosomes 1,

4, 13, 16, 18 and X. In addition, many high-level amplifications have been identified as predictive biomarkers, and numerous patient cohort studies have allowed clinicians to accurately characterize genetic changes that predict clinical outcomes [19–20] and precisely compare the genetic alterations between primary and metastatic lesions [15] or histotype-specific OC [21].

In the present study, we carried out an integrated analysis of ovarian cancer using, for the first time, a newly developed, high-resolution genome-wide CNV targeted array to identify CNV-driven genes with bioinformatic tools. The identified CNV-related differentially expressed genes may contribute to the distinct invasive/migratory capacities of OC and serve as potential biomarkers that can improve the accuracy of clinical interpretations and the effectiveness of therapeutics for OC.

RESULTS

Comparisons of CNV and LOH frequency between metastatic OC and normal ovarian epithelial tissues

All 4 samples showed chromosomal aberrations. There were, on average, 38.75 chromosomal arm aberrations per specimen among the ovarian tumours and 40.5 aberrations per specimen among the normal tissues ($P < 0.05$). There were ≥ 40 chromosomal arm aberrations in 100% (20/20) of the normal tissues and 25% (1/4) of the ovarian tumours. There was a similar percentage of LOH between the two groups (Table 1).

The genome-wide distributions of CNVs are shown in Figure 1. Most of the imbalances in both groups involved LOH. Recurrent, common genomic aberrations between the two groups were observed at several chromosomal intervals. Most notably, CNVs at 7q, 8q, 9q, 12q, 13q, 14q, 16q, 18q, 20q, Xp and Xq were observed in the two groups. The most common CNV regions in the OC samples compared with the normal samples involved both LOH regions, including Xq11.1 and Xp21.1, and amplifications, including 8q21.13, 8q11.21, and 8q23.3. Of these regions, the LOH at Xq11.1 and Xp21.1 and gains at 8q21.13 were novel, specific CNVs.

Validation of the CNV data in HO-8910 and HO-8910PM cell lines

To verify the different biological behaviours of the cellular models *in vitro*, a cell migration assay was performed. The results showed that the migration distances of the HO-8910PM and HO-8910 cell lines at 24 h were significantly different, with distances of $189.22 \pm 6.56 \mu\text{m}$ and $102.31 \pm 4.35 \mu\text{m}$, respectively ($t = 17.91$, $p < 0.01$) (Figure 2A). The difference in the

number of cells permeating the septum between the HO-8910PM (60.21 ± 1.78 cells) and HO-8910 (42.79 ± 2.35 cells) groups was significant ($t = 25.95$, $p < 0.01$) (Figure 2B).

In the HO-8910 versus HO-8910PM comparison, although the CNVs of both HO-8910 and HO-8910PM cells overlapped significantly, large regions differed between the two subclones. Segments of gain at 1p36.11, 1p34.3, 1p33, 1p32.1, 1q23.1, 1q32.3, 2q35, 3p26.2, 5p12, 8q21.13, 10p11.1, 10q23.33, 12q23.1, 12q23.3, 12q24.32, 17q12 and 20q12 appeared only in HO-8910PM cells (named “HO-8910PM-specific gain”), whereas segments of loss at 1p36.13, 1p13.3, 1q25.1, 2q22.3, 2q23.1, 2q24.2, 4q12, 5p12, 5q31.3, 6q16.2, 8q22.1, 8q24.11, 10p12.32, 10p12.1, 10p11.23, 10q26.11, 13q21.31, 14q11.2, 14q13.1 and 21q21.1 appeared only in HO-8910PM cells (named “HO-8910PM-specific loss”). The CNV profiles are shown in Figure 2C.

Screening of differentially expressed genes and enrichment analysis in HO-8910PM cells

Functional analysis by the Database for Annotation, Visualization and Integrated Discovery (DAVID) indicated that the proteins encoded by the “HO-8910PM-specific gain” genes (479 genes) are involved in the negative regulation of chondrocyte differentiation, respiratory chain complex IV assembly, myelination, the regulation of myelination, axon ensheathment and other processes (Figure 3A). A total of 479 “HO-8910PM-specific gain” genes were uploaded into the Kyoto Encyclopedia of Genes and Genomes (KEGG) database to conduct KEGG analysis. The significantly enriched KEGG terms were pathways in melanoma, the ECM-receptor interaction, focal adhesion, ABC transporters, adherens junctions, and others (Figure 3B). The proteins encoded by the “HO-8910PM-specific loss” genes (400 genes) displayed significant enrichment for xenobiotic glucuronidation, the negative regulation of cellular glucuronidation, flavonoid glucuronidation, glucuronosyl-transferase activity, cellular glucuronidation, and other terms (Figure 3C). The 400 genes were uploaded for KEGG analysis. The significantly enriched KEGG terms were pathways in ascorbate and aldarate metabolism, pentose and glucuronate interconversions, porphyrin and chlorophyll metabolism, other types of O-glycan biosynthesis, drug metabolism, and other terms (Figure 3D).

Construction of the protein-protein interaction (PPI) network and cluster identification

Among the “HO-8910PM-specific gain” and “HO-8910PM-specific loss” genes enriched in the KEGG

Table 1. Chromosomal arms affected by CNVs and LOH and the frequencies of CNVs and LOH in tissues.

Group	Sample ID	Chromosomal arm		Total number		Gain		Loss		LOH	
		NO.	Average	NO.	Average	NO.	Average	NO.	Average	NO.	Average
Cancer	LXM	39	38.75	206	178.5	187	141.75	19	36.75	216	197.25
	WXL	38		103		102		1		198	
	YLH	40		152		147		5		178	
	ZLQ	38		253		131		122		197	
Normal	GRY	41	40.5	167	186.5	42	39.5	125	147	165	155.5
	NDY	40		206		37		169		146	

database ($p > 0.05$), 71 were shared. To obtain protein interaction data, a human PPI dataset from the Search Tool for the Retrieval of Interacting Genes (STRING) database was applied to the 71 genes. The MCODE

algorithm in Cytoscape was used to identify highly interconnected regions or regions of high density in the network. In total, 54 nodes and 112 edges occurred in the PPI network. *GAB2* [22], *AKT1* [23], *EGFR* [24],

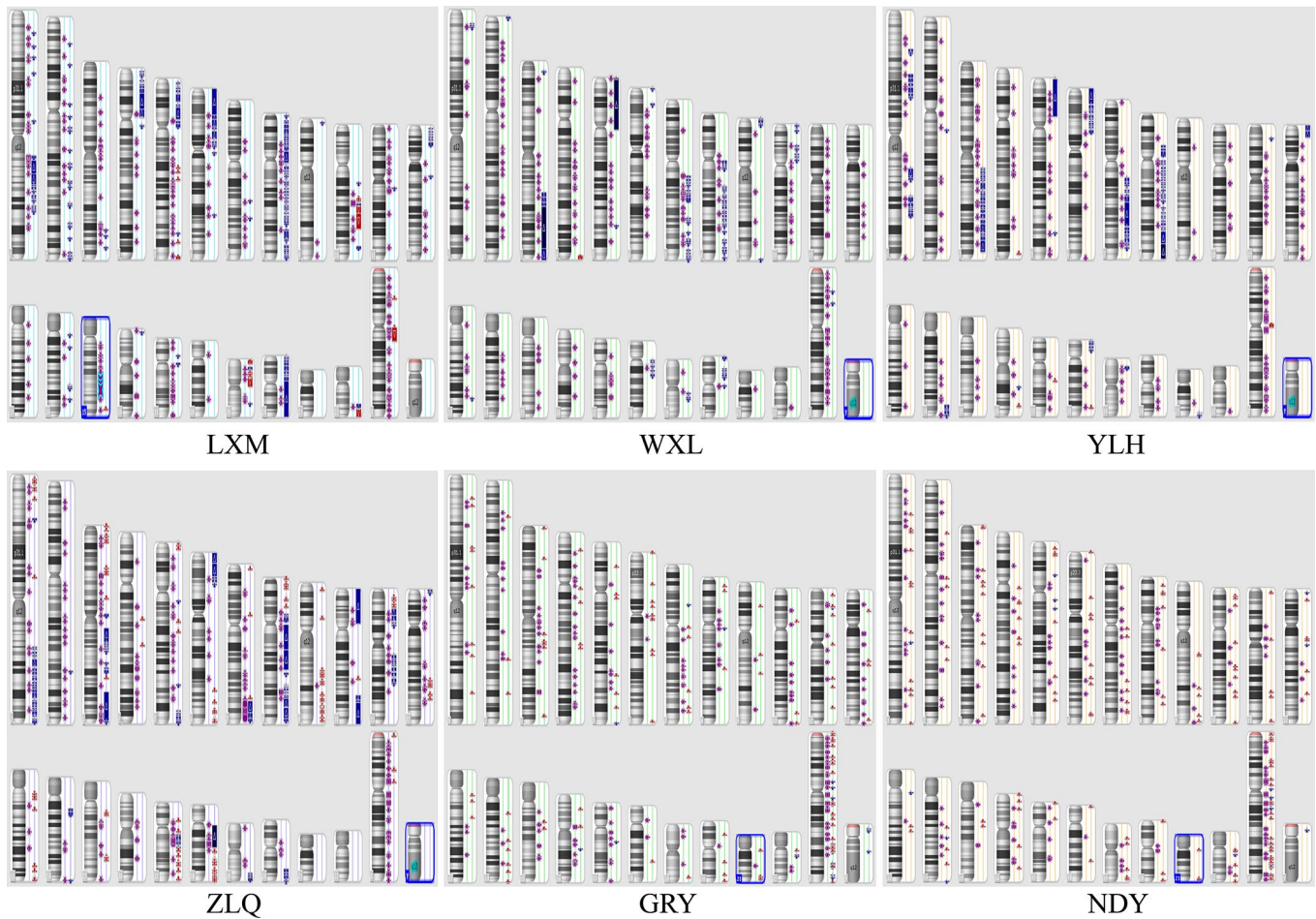


Figure 1. Illustration of the copy number state of all samples. Chromosomes 1 through 12 are shown in the upper panel (from left to right), chromosomes 13 through 22 are shown in the lower panel, and chromosomes X and Y are shown in the lower right panel. Six samples were included (LXM, WXL, YLH, and ZLQ: OC; and GRY and NDY: normal epithelial OC). Colour indicates copy number status (blue, duplication; red, deletion; purple, LOH); greater colour saturation indicates greater CNV.

CTNNB1 [25], *HRAS* [26], *ITGB7* [27], *COL6A1* [28], *COL6A3* [29], *UGT1A1* [30], *UGT1A10* [31], *UGT1A3* [32], *UGT1A4* [33], *UGT1A6* [34], *UGT1A7* [35], *UGT1A8* [36], and *UGT1A9* [37] were the top 16 genes with the highest connectivity degree (Figure 4).

Assessment of candidate gene expression and patient outcomes

To evaluate the prognostic values of the 16-gene signature selected by the PPI, the Kaplan-Meier plotter (KM plotter) was applied. Progression-free survival (PFS) for patients with OC was determined according to the low and high expression of the hub genes. The results showed that high *GAB2*, *AKT1*, *EGFR*, and *COL6A3* expression were associated with poor PFS for OC patients ($P < 0.05$). Additionally, high *UGT1A1* and *UGT1A8* expression were associated with improved PFS for OC patients ($P < 0.05$) (Figure 5). However, the

results also showed that the expression levels of *CTNNB1*, *HRAS*, *ITGB7*, *COL6A1*, *UGT1A10*, *UGT1A3*, *UGT1A4*, *UGT1A6*, *UGT1A7*, and *UGT1A9* did not correlate with PFS ($P > 0.05$).

Prognostic significance of *GAB2*, one of the genes of the 16-gene signature in relation to current clinical covariates

To investigate the prognostic significance of the 16-gene signature in association with stage and grade in all validation datasets, we chose *GAB2*, for which the most statistically significant differences had been identified, for univariate and multivariate Cox regression analyses. *GAB2* was a stronger predictor of PFS than grade and stage in both the univariate and multivariate analyses (HR 1.473, 95% CI 1.229-1.766, $P < 0.01$; and HR 1.423, 95% CI 1.989-2.047, $p = 0.003$ respectively; Table 2).

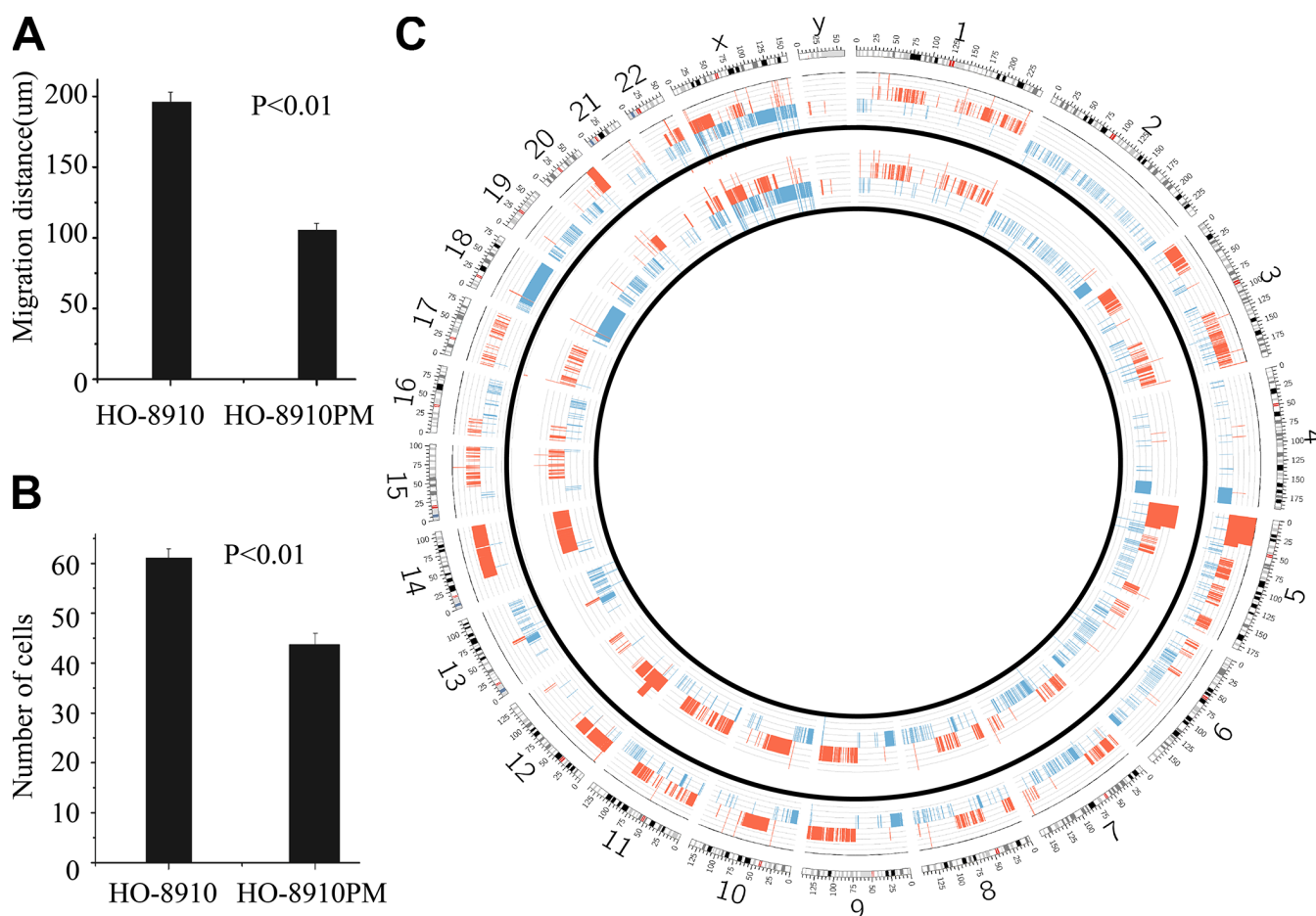


Figure 2. Different biological behaviours and CNVs in OC cell lines. The migration distance in the HO-8910 cell line was less than that in the HO-8910PM cell line ($p < 0.01$) (A). Cells were incubated on migration wells for 48 h, and the number of cells that migrated to the lower side of the filter was counted (B). The results are shown as the mean \pm standard deviation (SD) ($p < 0.01$ compared to the HO-8910 cell line). (C) Circos plot of the segmented CNVs in HO-8910PM (inner race) and HO-8910 (outer race) cell lines. Coloured bands expanding towards the centre or periphery of the diagram represent copy number losses or gains, respectively (red, gain; blue, loss).

TFs associated with the 6-gene signature

Four candidate gene-related TFs associated with OC, namely, RFX1, ATF3, CREB, and LHX3, were predicted with a PASTAA analysis ($p < 0.01$). The TF-target gene regulatory network was constructed by introducing the TF and target gene into Cytoscape software (Figure 6A). Relative to the corresponding expression in HO-8910 cells, RFX1, ATF3, and CREB, of a total 345 candidate TFs, were upregulated extensively in HO-8910PM cells, but there was no significant difference in LHX3 expression between the two cell lines (Figure 6B).

DISCUSSION

Previous studies [38–40] have demonstrated heterogeneity among OCs. The aim of the present study was

to compare overall CNVs and LOH across the entire genome using the limiting dilution method [41] to isolate and establish heterogeneous subclones of ovarian cancer tissues and cell lines. The results showed that the most common CNV regions in the OC samples compared with the normal samples were LOH regions, including Xq11.1 and Xp21.1, and amplification regions, including 8q21.13, 8q11.21, and 8q23.3 [42]. Among the CNVs, LOH at Xq11.1 and Xp21.1 and gains at 8q21.13 were novel, specific CNVs. These results suggest that unknown DNA repair genes might be involved in tumour metastasis [43]. However, the HO-8910-derived subclones differed extensively from the normal tissue. Different OC histotypes represented genetic disparities. We hypothesized that heterogeneity may preferentially evolve due to initial alterations in DNA followed by alterations in chromosomal copy number. In the present study, we analysed CNVs in

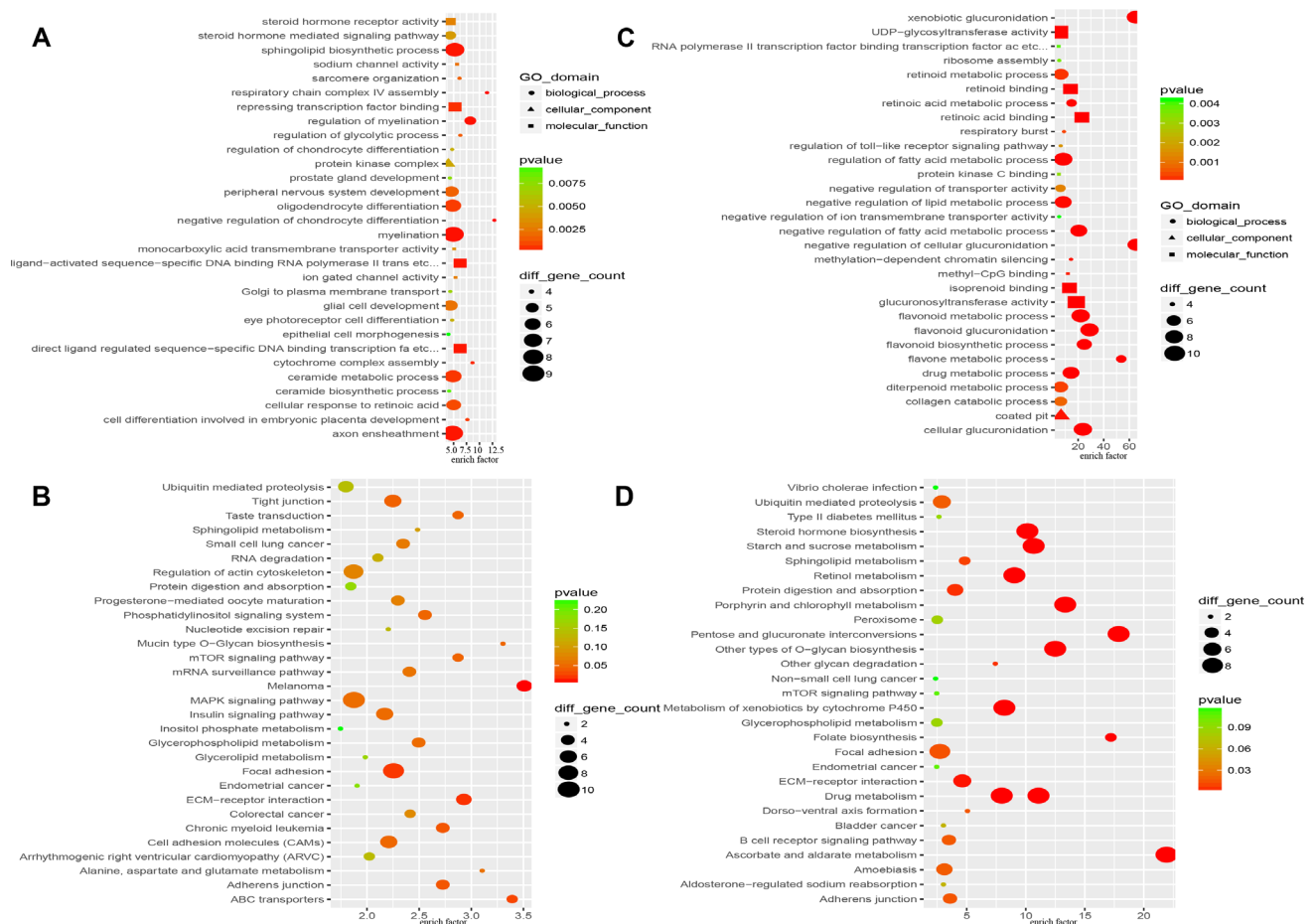


Figure 3. Functional enrichment analysis of “HO-8910PM-specific gain” and “HO-8910PM-specific loss” genes identified in CNV regions. (A) GO-based annotation was used for the functional enrichment analysis of genes with shared “HO-8910PM-specific gains” (479 genes). (B) KEGG pathway analysis of genes with shared “HO-8910PM-specific gains” (479 genes). (C) GO-based annotation was used for the functional enrichment analysis of genes with shared “HO-8910PM-specific loss” (400 genes) through DAVID. (D) KEGG pathway analysis of genes with shared “HO-8910PM-specific loss” (400 genes). Colour represents the $-\log$ of the P value for the significance of enrichment. Only annotations with significant P values < 0.05 are shown.

invasive/migratory models. Among the subclones, the HO-8910 and HO-8910PM cell lines, as a pair, serve as *in vitro* research models of OC metastasis. Two cell lines were validated in our previous studies [44–45]. Accordingly, the CNV observed at 8q21.13 between HO-8910PM cells and metastatic OC tissue might be cellular-phenotype related.

CNVs play important roles in the pathogenesis of various types of cancer, such as the CNVs of BRCA, which have been found to be associated with ovarian cancer [46] and breast cancer [47]. In the present study, 16 genes signature [48] with associated copy numbers and differential expression were acquired, of which 6 gene showed the same trends in CNV and were regarded as ovarian

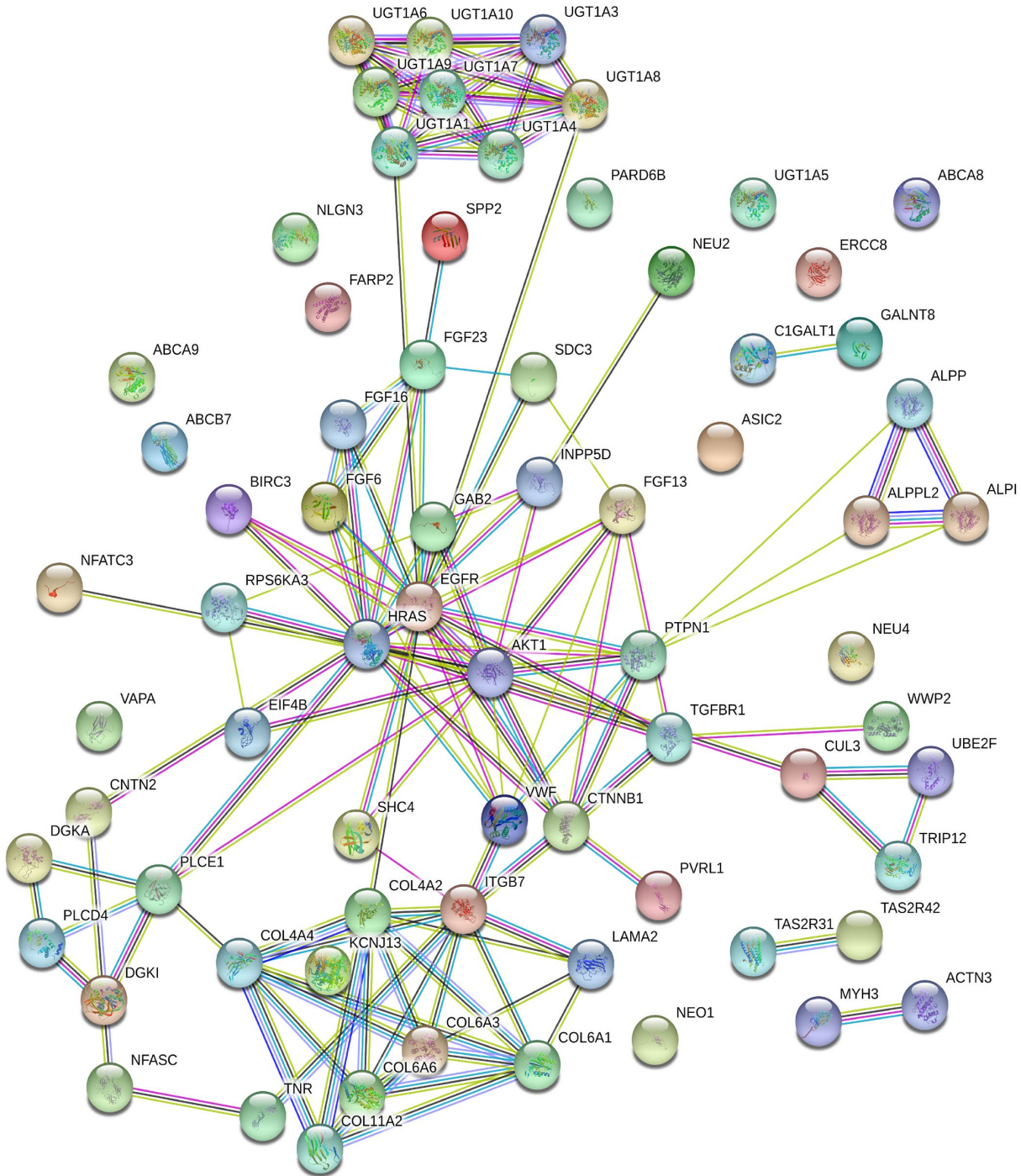


Figure 4. PPI network based on 71 genes. There are 54 nodes and 112 edges in the network. Nodes represent genes, and edges represent the interactions between genes.

cancer-related CNV-driven genes. GAB2 overexpression was associated with poor PFS for OC patients, which was in accordance with previous studies. Overexpression of GAB2 in ovarian cancer cells promotes tumour growth and angiogenesis by upregulating the expression of CXCL1, CXCL2 and CXCL8, which are IKK β -dependent [49]. Gab2 inhibits E-cadherin expression and enhances the expression of Zeb1, a transcription factor involved in epithelial-to-mesenchymal transition (EMT), and cell migration and invasion through the activation of the PI3K pathway [50]. Co-targeting the IKK β and PI3K pathways downstream of GAB2 might be a promising therapeutic strategy for ovarian cancer. AKT1 and EGFR play major roles in tumour progression and metastasis in ovarian cancer [51–52]. Davies found that AKT1 (E17K) mutations were effective therapeutic targets for AKT inhibitors [53], although combinations with other targeted agents may be required where activating oncogenic mutations of other proteins were present in the same tumour [54]. Furthermore, alterations in EGFR have been found to perturb enzyme efficacy and

proliferation in ovaries and impact susceptibility to OC [55]. COL6A3 was shown to be upregulated in ovarian cancer [56]. Sherman [57] found that the expression of COL6A3 was correlated with cisplatin resistance in ovarian cancer cell lines. Furthermore, highly or moderately differentiated ovarian tumours expressed lower levels of COL6A3 than poorly differentiated tumours, which indicated that the expression of COL6A3 was associated with the grade of the ovarian tumour [57]. There are no reports to date on the relationship between COL6A3 and the metastasis of ovarian cancer. COL6A3 may be a new biomarker for the metastasis of OC. However, UGT1A1 and UGT1A8 over-expression were associated with improved PFS in OC patients. UGT1A1, which has three different variants (UGT1A1*6, UGT1A1*27 and UGT1A1*28), mediates the glucuronidation of SN-38 and CYP3A4, which results in several pharmacologically inactive oxidation products. Homozygosity for UGT1A1*6 or heterozygosity for UGT1A1*6/*28 was associated with a high risk of severe absolute neutrophil count decrease or diarrhoea. In

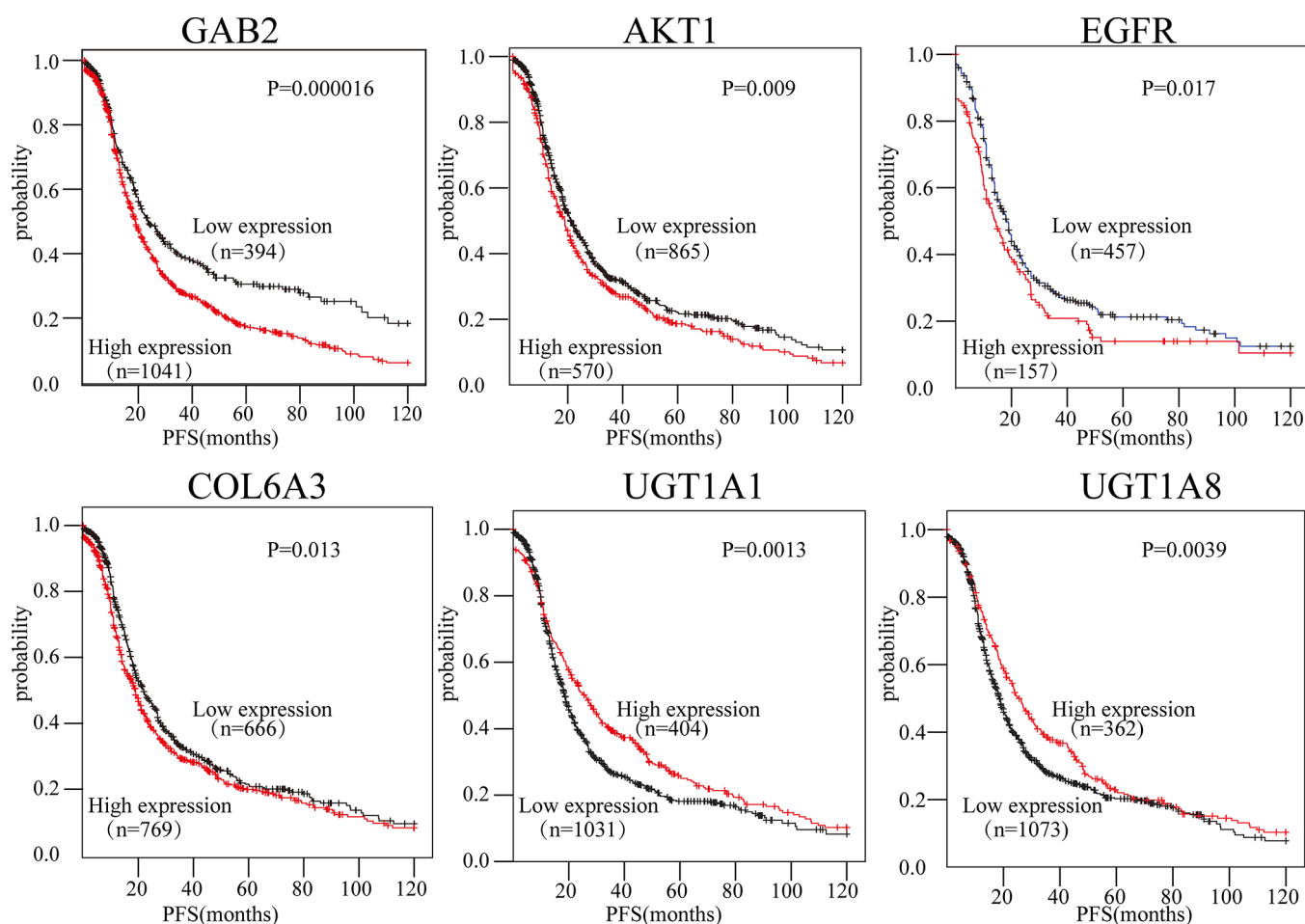


Figure 5. The expression of six genes predicts the prognosis of OC patients. The prognostic values of the six genes in OC patients were determined ($P < 0.05$).

Table 2. Univariate and multivariate Cox proportional hazard regression analyses in all combined validation datasets.

Variable	Univariate analysis			Multivariate analysis		
	HR	95% CI	P value	HR	95% CI	P value
pathology	0.604	0.424-0.860	0.005	0.748	0.618-0.904	0.057
Stage	1.467	1.190-1.806	<0.01	1.347	1.088-1.688	0.006
Grade	0.724	0.545-0.962	0.026	0.795	0.597-1.058	0.115
GAB2	1.473	1.229-1.766	<0.01	1.423	0.989-2.047	0.003

Current clinicopathological factors in ovarian cancer including pathology, stage and grade analyzed in association with the GAB2 gene signature in all combined validation datasets. (HR) hazard ratio; (CI) confident interval.

addition to UGT1A1*28, UGT1A1*6 might be a key candidate for determining the dose of combination chemotherapy with irinotecan and cisplatin [58]. The presence of UGT1A1*28 results in an increased risk of ovarian cancer. UGT1A1*28 is associated with mucinous carcinoma and may have a role in the formation of specific histologic sub-groups. It is a potential marker to be considered when planning ovarian cancer chemotherapy [59]. There are no reports to date regarding UGT1A8 in ovarian cancer. There is one study of recombinant human UDP-glucuronosyltransferases (UGTs), including UGT1A1, but Zhou [60] found that UGT1A8 gene polymorphisms can affect the activity of the UDP glucuronosyltransferase enzyme, which may influence the elimination of mycophenolate mofetil in different patients. The 6 CNV-driven genes identified in

the present study may be potential markers for ovarian cancer.

In the transcriptional regulatory network, RFX1, ATF3, CREB, and LHX3 were predicted as OC candidate gene-related TFs in the PASTAA analysis. Only RFX1, ATF3, and CREB showed two-fold increases in expression in HO-8910PM/HO-8910 cells, which was validated with protein/DNA arrays. Consistent with these results, Subbiah reported that CREB, an important TF for neurotrophin activity, employed signalling pathways mediated by PI3-kinase and p38 MAPK, whereas Akt, the downstream component of the PI3-kinase pathway, is known to regulate the covalent modification of cytosolic proteins, such as glycogen synthase and the proapoptotic protein BAD, in

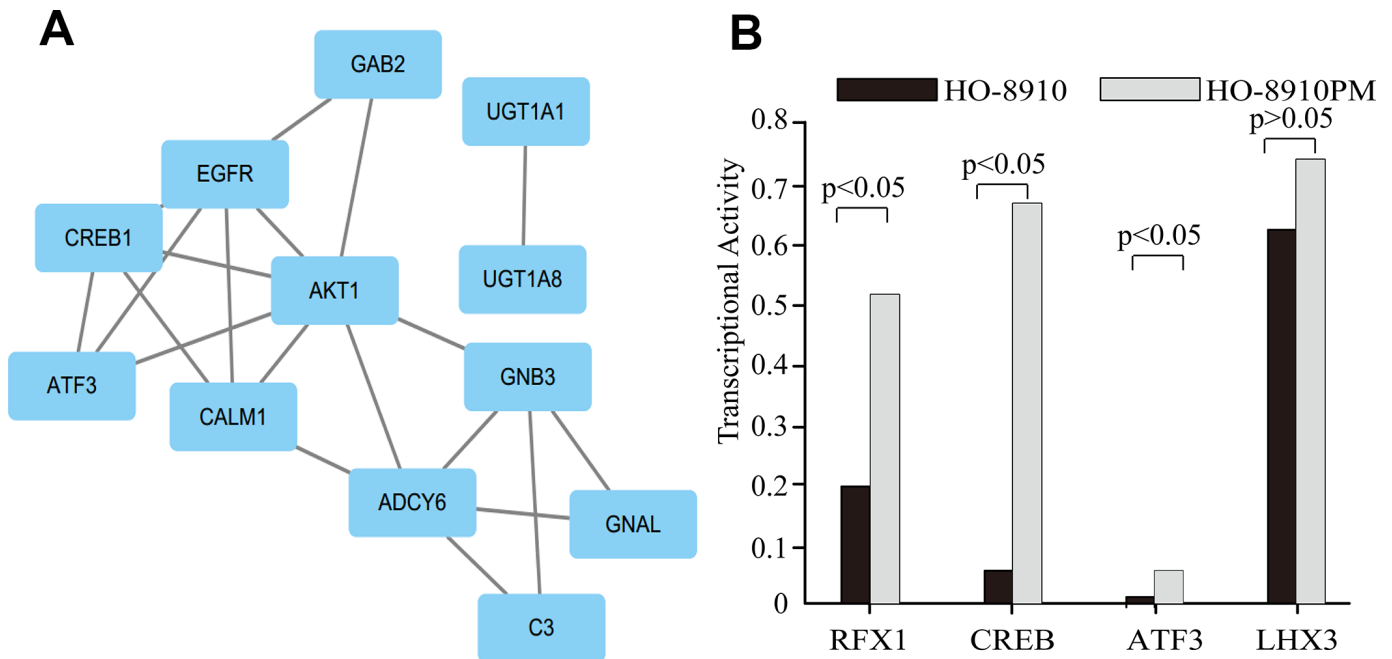


Figure 6. The target genes and their predicted TFs. (A) The clusters identified in the PPI network containing the target genes and their predicted TFs. **(B)** The transcriptional activities of four TFs.

pheochromocytoma (PC12) cells [61]. The phosphoinositide 3-kinase protein kinase B (PI3K-Akt) signalling pathway was involved in the formation and progression of many malignancies due to genetic alterations in their components or the activation of upstream cell surface receptors [62]. Future studies are needed to explore the implications of each of signalling pathway on CREB-responsive genes important for cell cycle regulation, survival, and differentiation in OC. It has been observed that COL6A3 acts as an oncogene in cancer and that the antagonism of COL6A3 could be developed as an effective therapeutic treatment for gastric cancer [63]. The number of cells that expressed COL6A3 relative to normal cells, Akt and PI3K were markedly decreased. COL6A3 gene silencing inhibits gastric cancer cell proliferation, migration, and invasion and promotes apoptosis through the PI3K-Akt signalling pathways [64]. The present need to be confirmed before the clinical application of COL6A3 and the CREB and PI3K-Akt signalling pathways in patients with OC. However, the association between other hub genes and OC has not been widely reported and needs further investigation.

In summary, we systematically analysed the functions of altered genes in OC cell line models with distinct invasive/migratory capacities. Data on copy number diversity were integrated with clinical outcomes and DNA/protein expression to facilitate the search for potential therapeutic targets. We hypothesize that clone-specific functional and genetic profiling will be helpful methods for identifying new molecular pathways underlying cancer and new biomarkers for clinical applications. This information will not only reveal the heterogeneity of OC at different developmental stages but also elucidate other factors that contribute to cancer-related deaths, such as genes that promote invasion/migration.

MATERIALS AND METHODS

Patients

The samples analysed in this study were tissue bank samples from 4 OC patients with lymph node metastasis and samples of normal ovarian surface epithelia from 2 non-OC patients the Fujian Maternity and Children Health Hospital (Fujian, China). Tissues were collected after the time of surgery. Four patients with metastatic OC who received surgical treatment between May 2013 and January 2015 were selected. Metastatic OC was identified intraoperatively and postoperatively. The patients' ages ranged between 55 and 60 years. The postoperative pathology revealed 2 serous adenocarcinomas, a mucinous adenocarcinoma, and a serous cystadenocarcinoma. Normal ovarian epithelial tissue

was obtained from two patients that had undergone bilateral appendage removal due to other benign gynaecological diseases. The ages of these 2 patients were 39 years and 47 years. All participants provided written informed consent, and all study protocols were approved by the Ethics Committee of the Fujian Maternity and Children Health Hospital (Fujian, China) (approval number 2013004). All methods of data collection and analysis were performed in accordance with relevant guidelines and regulations and with appropriate quality control.

CNV assay

Tumour samples were obtained from each patient, and DNA was extracted using a QIAamp DNA Blood Midi Kit (Qiagen, Duesseldorf, Germany) following the manufacturer's instructions. The CNVs were detected with a CytoScan HD microarray platform (Affymetrix, Santa Clara, CA, USA) and a high-density chip that contained 2,636,550 probes. All samples passed initial quality control. The array data were analysed using the Chromosome Analysis Suite (ChAS) software package [65], and annotations were performed with the Genome Reference Consortium (GRC) human reference genome version GRCh37 (hg19). The data were filtered such that only those regions larger than 50 kb comprising at least 25 contiguous markers were retained.

Data analysis

To calculate the CNV, the data were normalized to baseline reference intensities using 270 HapMap samples and data from 90 healthy normal individuals included in the software. The Hidden Markov Model (HMM) (available within the software package) was used to determine the copy number states and their breakpoints. The thresholds of \log_2 ratio ≥ 1.5 and ≤ -1.5 (as suggested by the software) were used to categorize the altered regions as CNV gains (amplifications) and copy number losses (deletions), respectively.

To prevent the detection of false-positive CNVs arising due to inherent microarray "noise", only alterations that involved at least 25 consecutive probes and that were >50 kb in length were considered in the analysis of gains or losses in our study. Amplifications and deletions were analysed separately. The detected CNVs were evaluated separately in terms of frequency and length. To exclude aberrations representing common, normal CNVs, all the identified CNVs were compared with those reported in the Database of Genomic Variants (DGV, <http://projects.tcag.ca/variation/>).

To identify genes involved in CNVs, the UCSC (<http://genome.ucsc.edu>), Ensemble (<http://www.ensembl.org>),

and BioGPS databases (<http://biogps.org>) were queried. The gene annotations and overlaps were determined using the human genome build 19 (hg19) and several widely used online databases (Ensembl: <http://www.ensembl.org>; UCSC: <http://genome.ucsc.edu>; and NetAffx: <http://www.affymetrix.com>).

For the LOH analysis, the LOH algorithm in the genotyping console 2.0 was used. Regions of LOH/copy number LOH (cnLOH) that were >3 Mb were identified and analysed further.

Pathway and functional enrichment analyses

To investigate the biological characteristics of the overlapping genes in the detected CNV regions, GO and KEGG pathway enrichment analyses were performed using DAVID [66, 67]. The cut off criterion was set as $P < 0.05$.

Cell lines and cell cultures

The OC cell line HO-8910 and its metastatic equivalent, HO-8910PM [68], were purchased from the Type Culture Collection Center of the Chinese Academy of Science (Shanghai, China). All cell lines were cultured in Dulbecco's modified Eagle's medium (DMEM) (Gibco; Thermo Fisher Scientific, Inc., Waltham, MA, United States) supplemented with 10% foetal bovine serum (Gibco), 1% penicillin and 1% streptomycin (100 IU/ml) in a 37°C incubator with 5% CO₂.

Cell scratch assay

The horizontal migration of cells was assessed with a scratch assay performed according to a previous report [69] with slight modifications. Cells were seeded at a density of 5.0×10^5 cells/well and imaged at 40× magnification with an Olympus IX70 inverted fluorescence microscope (Olympus Corporation, Japan) at 0 and 24 h post-scratching. Image-Pro Express C software 5.1 (Olympus Corporation) was used to measure the change in cell distance between scratches. The average horizontal migration rate was calculated using the following formula: (width at 0 h - width at 24 h) / width at 0 h × 100.

Transwell chamber assay

The invasive capacity of the cell lines was determined using a Matrigel invasion chamber assay. Cells were seeded at a density of 5.0×10^5 cells/well. The number of cells on the underside of the filter was determined by counting cells in five random fields from three filters for each treatment at 200× magnification with an inverted microscope (Olympus Corporation).

PPI network construction and cluster identification

PPI networks may represent molecular complexes. The PPI network of the genes was constructed using the STRING database (<https://string-db.org>). Upon entering a single protein name, multiple names or an amino acid sequence in the STRING website, the STRING resource can construct a network of protein interactions. The network view summarizes the network of the predicted associations for a particular group of proteins. The network nodes represent proteins, and edges represent the predicted functional associations. Additionally, in the legend section, a list of inputs is shown, and the predicted associations are shown in a list below the input, sorted by score. Subsequently, the results can be visualized using Cytoscape software. The cutoff criterion of the confidence score was set as > 0.7 . In addition, the molecular complex in the global PPI network was obtained with MCODE. The screening options were set as follows: degree cutoff = 2, node score cutoff = 0.2, k-core = 2, and max. depth = 100.

Survival analysis

The KM plotter is a web tool that predicts the effect of genes on survival (<http://kmplot.com/analysis/index.php?p=background>). After entering the genes of interest into the website, we divided the patients into two groups according to the expression level of each gene and statistically analysed survival rate. Univariate and multivariate Cox proportional hazard regression analyses were performed to evaluate independent prognostic factors associated with survival. The gene signature, pathology, tumour grade, and FIGO stage were employed as covariates. The hazard ratio (HR) with 95% CIs and the log-rank P value were calculated and shown.

Prediction of TFs

The relevant TFs of the differentially expressed genes were predicted based on the PASTAA analysis [70]. The p value calculated by the hypergeometric test was used to assess the significance of the overlap between each OC gene and the predicted target of the TF. Next, a TRAP analysis was performed to predict the affinity relationship between the gene and the relevant TF. The TFs and the differentially expressed genes were introduced into Cytoscape software to construct a gene-TF coexpression network.

Nuclear and cytoplasmic protein extraction

Nuclear and cytoplasmic proteins were extracted from adherent cells at 70–90% confluence according the instructions provided with the NuCLEAR™ Extraction Kit (Sigma, United States). In summary, the cells were

rinsed with fresh phosphate-buffered saline (PBS), the appropriate amounts of reagents were added to the particular packed-cell volume, the cells were lysed, and the cytoplasmic and nuclear proteins were isolated by gradient centrifugation. Protein concentrations were quantitated with a BCATM assay kit from Pierce (United States).

Protein/DNA arrays

HO-8910 and HO-8910PM cell cultures were screened for TFs using the TranSignal Protein/DNA Array (Panomics, United States) following the manufacturer's protocol. Briefly, proteins were isolated as described above, and nuclear extracts (25 µg) were incubated with the provided biotin-DNA probe mix for 30 minutes. Protein-DNA complexes were isolated with 2% agarose gel electrophoresis. The proteins were eliminated from the complex, and the biotin-DNA was hybridized to the membranes containing the consensus binding sequences of the TFs. Next, the membranes were incubated with streptavidin-alkaline phosphatase conjugate. Signals of the hybridized probes were visualized using the chemiluminescent imaging system provided with the TranSignal Protein/DNA Array Kit and exposed to X-ray film [71]. Using the expression in HO-8910 cells as the benchmark, a two-fold increase or decrease in expression in HO-8910PM/HO-8910 cells was considered significant. Experiments were performed in duplicate.

Statistical analysis

Statistical analysis of the data was performed with SPSS 17.0 software (SPSS, Chicago, Illinois, USA). The data are expressed as the means ± standard errors of the mean (SEM). The significance of differences in values was evaluated through analysis of variance (ANOVA) or an unpaired two-tailed Student's t-test. A P value < 0.05 was considered to indicate a significant difference. All experiments were repeated at least three times.

ACKNOWLEDGMENTS

The authors would like to thank Mrs Xiaodan Mao, Mr. Binhua Dong, Mrs Fen Lin and Miss Yuqin Gao for their excellent assistance in this work.

CONFLICTS OF INTEREST

The authors declare that they have no Conflicts of interests.

FUNDING

This study was supported in part by grant 2014J01278 from the Natural Science Foundation of Fujian

Province, China; grant 2014-ZQN-ZD-5 from the Young and Middle-Aged Talent Training Project of Fujian Province, China; and grant 2014-2-5 from the Youth Scientific Research Subject of Fujian Province, China.

REFERENCES

1. Jemal A, Bray F, Center MM, Ferlay J, Ward E, Forman D. Global cancer statistics. *CA Cancer J Clin.* 2011; 61:69–90.
<https://doi.org/10.3322/caac.20107>
PMID:[21296855](https://pubmed.ncbi.nlm.nih.gov/21296855/)
2. Siegel R, Desantis C, Jemal A. Colorectal cancer statistics, 2014. *CA Cancer J Clin.* 2014; 64:104–17.
<https://doi.org/10.3322/caac.21220>
PMID:[24639052](https://pubmed.ncbi.nlm.nih.gov/24639052/)
3. Lengyel E. Ovarian cancer development and metastasis. *Am J Pathol.* 2010; 177:1053–64.
<https://doi.org/10.2353/ajpath.2010.100105>
PMID:[20651229](https://pubmed.ncbi.nlm.nih.gov/20651229/)
4. Greaves M, Maley CC. Clonal evolution in cancer. *Nature.* 2012; 481:306–13.
<https://doi.org/10.1038/nature10762> PMID:[22258609](https://pubmed.ncbi.nlm.nih.gov/22258609/)
5. Heppner GH. Tumor heterogeneity. *Cancer Res.* 1984; 44:2259–65. PMID:[6372991](https://pubmed.ncbi.nlm.nih.gov/6372991/)
6. Conrad DF, Pinto D, Redon R, Feuk L, Gokcumen O, Zhang Y, Aerts J, Andrews TD, Barnes C, Campbell P, Fitzgerald T, Hu M, Ihm CH, et al. Origins and functional impact of copy number variation in the human genome. *Nature.* 2010; 464:704–12.
<https://doi.org/10.1038/nature08516> PMID:[19812545](https://pubmed.ncbi.nlm.nih.gov/19812545/)
7. Beckmann JS, Estivill X, Antonarakis SE. Copy number variants and genetic traits: closer to the resolution of phenotypic to genotypic variability. *Nat Rev Genet.* 2007; 8:639–46.
<https://doi.org/10.1038/nrg2149> PMID:[17637735](https://pubmed.ncbi.nlm.nih.gov/17637735/)
8. Bollig-Fischer A, Michelhaugh SK, Wijesinghe P, Dyson G, Kruger A, Palanisamy N, Choi L, Alesh B, Ali-Fehmi R, Mittal S. Cytogenomic profiling of breast cancer brain metastases reveals potential for repurposing targeted therapeutics. *Oncotarget.* 2015; 6:14614–24.
<https://doi.org/10.18632/oncotarget.3786>
PMID:[25970776](https://pubmed.ncbi.nlm.nih.gov/25970776/)
9. Cancer Genome Atlas Research Network. Integrated genomic analyses of ovarian carcinoma. *Nature.* 2011; 474:609–15.
<https://doi.org/10.1038/nature10166> PMID:[21720365](https://pubmed.ncbi.nlm.nih.gov/21720365/)
10. Sonoda G, Palazzo J, du Manoir S, Godwin AK, Feder M, Yakushiji M, Testa JR. Comparative genomic hybridization detects frequent overrepresentation of chromosomal material from 3q26, 8q24, and 20q13 in

- human ovarian carcinomas. *Genes Chromosomes Cancer*. 1997; 20:320–28.
[https://doi.org/10.1002/\(SICI\)1098-2264\(199712\)20:4<320::AID-GCC2>3.0.CO;2-3](https://doi.org/10.1002/(SICI)1098-2264(199712)20:4<320::AID-GCC2>3.0.CO;2-3)
 PMID:9408747
11. Gray JW, Suzuki S, Kuo WL, Polikoff D, Deavers M, Smith-McCune K, Berchuck A, Pinkel D, Albertson D, Mills GB. Specific keynote: genome copy number abnormalities in ovarian cancer. *Gynecol Oncol*. 2003; 88:S16–21.
<https://doi.org/10.1006/gyno.2002.6677>
 PMID:12586079
 12. Etemadmoghadam D, deFazio A, Beroukhi R, Mermel C, George J, Getz G, Tothill R, Okamoto A, Raeder MB, Harnett P, Lade S, Akslen LA, Tinker AV, et al. Integrated genome-wide DNA copy number and expression analysis identifies distinct mechanisms of primary chemoresistance in ovarian carcinomas. *Clin Cancer Res*. 2009; 15:1417–27.
<https://doi.org/10.1158/1078-0432.CCR-08-1564>
 PMID:19193619
 13. Kim SW, Kim JW, Kim YT, Kim JH, Kim S, Yoon BS, Nam EJ, Kim HY. Analysis of chromosomal changes in serous ovarian carcinoma using high-resolution array comparative genomic hybridization: potential predictive markers of chemoresistant disease. *Genes Chromosomes Cancer*. 2007; 46:1–9.
<https://doi.org/10.1002/gcc.20384> PMID:17044060
 14. Goringe KL, Jacobs S, Thompson ER, Sridhar A, Qiu W, Choong DY, Campbell IG. High-resolution single nucleotide polymorphism array analysis of epithelial ovarian cancer reveals numerous microdeletions and amplifications. *Clin Cancer Res*. 2007; 13:4731–39.
<https://doi.org/10.1158/1078-0432.CCR-07-0502>
 PMID:17699850
 15. Malek JA, Mery E, Mahmoud YA, Al-Azwani EK, Roger L, Huang R, Jouve E, Lis R, Thiery JP, Querleu D, Rafii A. Copy number variation analysis of matched ovarian primary tumors and peritoneal metastasis. *PLoS One*. 2011; 6:e28561.
<https://doi.org/10.1371/journal.pone.0028561>
 PMID:22194851
 16. Goringe KL, George J, Anglesio MS, Ramakrishna M, Etemadmoghadam D, Cowin P, Sridhar A, Williams LH, Boyle SE, Yanaiharu N, Okamoto A, Urashima M, Smyth GK, et al. Copy number analysis identifies novel interactions between genomic loci in ovarian cancer. *PLoS One*. 2010; 5:e11408.
<https://doi.org/10.1371/journal.pone.0011408>
 PMID:20844748
 17. Wrzeszczynski KO, Varadan V, Byrnes J, Lum E, Kamalakaran S, Levine DA, Dimitrova N, Zhang MQ, Lucito R. Identification of tumor suppressors and oncogenes from genomic and epigenetic features in ovarian cancer. *PLoS One*. 2011; 6:e28503.
<https://doi.org/10.1371/journal.pone.0028503>
 PMID:22174824
 18. Lee JY, Yoon JK, Kim B, Kim S, Kim MA, Lim H, Bang D, Song YS. Tumor evolution and intratumor heterogeneity of an epithelial ovarian cancer investigated using next-generation sequencing. *BMC Cancer*. 2015; 15:85.
<https://doi.org/10.1186/s12885-015-1077-4>
 PMID:25881093
 19. Wang ZC, Birkbak NJ, Culhane AC, Drapkin R, Fatima A, Tian R, Schwede M, Alsop K, Daniels KE, Piao H, Liu J, Etemadmoghadam D, Miron A, et al. Profiles of genomic instability in high-grade serous ovarian cancer predict treatment outcome. *Clin Cancer Res*. 2012; 18:5806–15.
<https://doi.org/10.1158/1078-0432.CCR-12-0857>
 PMID:22912389
 20. Engler DA, Gupta S, Growdon WB, Drapkin RI, Nitta M, Sargent PA, Allred SF, Gross J, Deavers MT, Kuo WL, Karlan BY, Rueda BR, Orsulic S, et al. Genome wide DNA copy number analysis of serous type ovarian carcinomas identifies genetic markers predictive of clinical outcome. *PLoS One*. 2012; 7:e30996.
<https://doi.org/10.1371/journal.pone.0030996>
 PMID:22355333
 21. Huang RY, Chen GB, Matsumura N, Lai HC, Mori S, Li J, Wong MK, Konishi I, Thiery JP, Goh L. Histotype-specific copy-number alterations in ovarian cancer. *BMC Med Genomics*. 2012; 5:47.
<https://doi.org/10.1186/1755-8794-5-47>
 PMID:23078675
 22. Adams SJ, Aydin IT, Celebi JT. GAB2—a scaffolding protein in cancer. *Mol Cancer Res*. 2012; 10:1265–70.
<https://doi.org/10.1158/1541-7786.MCR-12-0352>
 PMID:22871571
 23. Elzaat M, Herman L, Legois B, Léger T, Todeschini AL, Veitia RA. High-throughput Exploration of the Network Dependent on AKT1 in Mouse Ovarian Granulosa Cells. *Mol Cell Proteomics*. 2019; 18:1307–19.
<https://doi.org/10.1074/mcp.RA119.001461>
 PMID:30992313
 24. Nicholson RI, Gee JM, Harper ME. EGFR and cancer prognosis. *Eur J Cancer*. 2001 (Suppl 4); 37:S9–15.
[https://doi.org/10.1016/S0959-8049\(01\)00231-3](https://doi.org/10.1016/S0959-8049(01)00231-3)
 PMID:11597399
 25. Terakawa J, Serna VA, Taketo MM, Daikoku T, Suarez AA, Kurita T. Ovarian insufficiency and CTNNB1 mutations drive malignant transformation of endometrial hyperplasia with altered PTEN/PI3K

- activities. *Proc Natl Acad Sci USA*. 2019; 116:4528–37. <https://doi.org/10.1073/pnas.1814506116> PMID:30782821
26. Shukla A, Dahiya S, Onteru SK, Singh D. Differentially expressed miRNA-210 during follicular-luteal transition regulates pre-ovulatory granulosa cell function targeting HRas and EFNA3. *J Cell Biochem*. 2018; 119:7934–43. <https://doi.org/10.1002/jcb.26508> PMID:29131373
 27. Neri P, Ren L, Azab AK, Brentnall M, Gratton K, Klimowicz AC, Lin C, Duggan P, Tassone P, Mansoor A, Stewart DA, Boise LH, Ghobrial IM, et al. Integrin β -mediated regulation of multiple myeloma cell adhesion, migration, and invasion. *Blood*. 2011; 117:6202–13. <https://doi.org/10.1182/blood-2010-06-292243> PMID:21474670
 28. Hou T, Tong C, Kazobinka G, Zhang W, Huang X, Huang Y, Zhang Y. Expression of COL6A1 predicts prognosis in cervical cancer patients. *Am J Transl Res*. 2016; 8:2838–44. PMID:27398167
 29. Liu W, Li L, Ye H, Tao H, He H. Role of COL6A3 in colorectal cancer. *Oncol Rep*. 2018; 39:2527–36. <https://doi.org/10.3892/or.2018.6331> PMID:29620224
 30. Takaoka Y, Takeuchi A, Sugano A, Miura K, Ohta M, Suzuki T, Kobayashi D, Kimura T, Sato J, Ban N, Nishio H, Sakaeda T. Establishment of the experimental procedure for prediction of conjugation capacity in mutant UGT1A1. *PLoS One*. 2019; 14:e0225244. <https://doi.org/10.1371/journal.pone.0225244> PMID:31730632
 31. Pawlowska M, Chu R, Fedejko-Kap B, Augustin E, Mazerska Z, Radomska-Pandya A, Chambers TC. Metabolic transformation of antitumor acridinone C-1305 but not C-1311 via selective cellular expression of UGT1A10 increases cytotoxic response: implications for clinical use. *Drug Metab Dispos*. 2013; 41:414–21. <https://doi.org/10.1124/dmd.112.047811> PMID:23160818
 32. Yilmaz L, Borazan E, Aytekin T, Baskonus I, Aytekin A, Oztuzcu S, Bozdogan Z, Balik A. Increased UGT1A3 and UGT1A7 expression is associated with pancreatic cancer. *Asian Pac J Cancer Prev*. 2015; 16:1651–55. <https://doi.org/10.7314/APJCP.2015.16.4.1651> PMID:25743847
 33. Lan B, Ma F, Han M, Chen S, Wang W, Li Q, Fan Y, Luo Y, Cai R, Wang J, Yuan P, Zhang P, Li Q, et al. The effect of polymorphism in UGT1A4 on clinical outcomes of adjuvant tamoxifen therapy for patients with breast cancer in China. *Clin Breast Cancer*. 2019; 19:e370–75. <https://doi.org/10.1016/j.clbc.2018.12.009> PMID:30630678
 34. Kua LF, Ross S, Lee SC, Mimura K, Kono K, Goh BC, Yong WP. UGT1A6 polymorphisms modulated lung cancer risk in a Chinese population. *PLoS One*. 2012; 7:e42873. <https://doi.org/10.1371/journal.pone.0042873> PMID:22912755
 35. Han SX, Wang L, Wu DQ. The association between UGT1A7 polymorphism and cancer risk: a meta-analysis. *Cancer Epidemiol*. 2012; 36:e201–06. <https://doi.org/10.1016/j.canep.2012.02.004> PMID:22402308
 36. Bao L, Zhang Y, Wang J, Wang H, Dong N, Su X, Xu M, Wang X. Variations of chromosome 2 gene expressions among patients with lung cancer or non-cancer. *Cell Biol Toxicol*. 2016; 32:419–35. <https://doi.org/10.1007/s10565-016-9343-z> PMID:27301951
 37. Girard H, Butler LM, Villeneuve L, Millikan RC, Sinha R, Sandler RS, Guillemette C. UGT1A1 and UGT1A9 functional variants, meat intake, and colon cancer, among Caucasians and African-Americans. *Mutat Res*. 2008; 644:56–63. <https://doi.org/10.1016/j.mrfmmm.2008.07.002> PMID:18675828
 38. Boesch M, Zeimet AG, Reimer D, Schmidt S, Gastl G, Parson W, Spoeck F, Hatina J, Wolf D, Sopper S. The side population of ovarian cancer cells defines a heterogeneous compartment exhibiting stem cell characteristics. *Oncotarget*. 2014; 5:7027–39. <https://doi.org/10.18632/oncotarget.2053> PMID:25216521
 39. Davis SJ, Sheppard KE, Pearson RB, Campbell IG, Goringe KL, Simpson KJ. Functional analysis of genes in regions commonly amplified in high-grade serous and endometrioid ovarian cancer. *Clin Cancer Res*. 2013; 19:1411–21. <https://doi.org/10.1158/1078-0432.CCR-12-3433> PMID:23362323
 40. Khalique L, Ayhan A, Weale ME, Jacobs IJ, Ramus SJ, Gayther SA. Genetic intra-tumour heterogeneity in epithelial ovarian cancer and its implications for molecular diagnosis of tumours. *J Pathol*. 2007; 211:286–95. <https://doi.org/10.1002/path.2112> PMID:17154249
 41. Bai H, Li H, Li W, Gui T, Yang J, Cao D, Shen K. The PI3K/AKT/mTOR pathway is a potential predictor of distinct invasive and migratory capacities in human ovarian cancer cell lines. *Oncotarget*. 2015; 6:25520–32. <https://doi.org/10.18632/oncotarget.4550> PMID:26267321

42. Parris TZ, Rönnerman EW, Engqvist H, Biermann J, Truvé K, Nemes S, Forssell-Aronsson E, Solinas G, Kovács A, Karlsson P, Helou K. Genome-wide multi-omics profiling of the 8p11-p12 amplicon in breast carcinoma. *Oncotarget*. 2018; 9:24140–54. <https://doi.org/10.18632/oncotarget.25329> PMID:[29844878](https://pubmed.ncbi.nlm.nih.gov/29844878/)
43. Wang P, Shan L, Xue L, Zheng B, Ying J, Lu N. Genome wide copy number analyses of superficial esophageal squamous cell carcinoma with and without metastasis. *Oncotarget*. 2017; 8:5069–80. <https://doi.org/10.18632/oncotarget.13847> PMID:[27974698](https://pubmed.ncbi.nlm.nih.gov/27974698/)
44. Sun P, Jiang Z, Chen X, Xue L, Mao X, Ruan G, Song Y, Mustea A. Decreasing the ratio of matriptase/HAI-1 by downregulation of matriptase as a potential adjuvant therapy in ovarian cancer. *Mol Med Rep*. 2016; 14:1465–74. <https://doi.org/10.3892/mmr.2016.5435> PMID:[27356668](https://pubmed.ncbi.nlm.nih.gov/27356668/)
45. Sun PM, Wei LH, Sehoul J, Denkert C, Zhao D, Gao M, Sun XL, Lichtenegger W. Role of estrogen receptor-related receptors alpha, beta and gamma in ovarian cancer cells. *Zhonghua Fu Chan Ke Za Zhi*. 2005; 40:544–48. PMID:[16202294](https://pubmed.ncbi.nlm.nih.gov/16202294/)
46. Minucci A, De Paolis E, Concolino P, De Bonis M, Rizza R, Canu G, Scaglione GL, Mignone F, Scambia G, Zuppi C, Capoluongo E. Competitive PCR-High Resolution Melting Analysis (C-PCR-HRMA) for large genomic rearrangements (LGRs) detection: A new approach to assess quantitative status of BRCA1 gene in a reference laboratory. *Clin Chim Acta*. 2017; 470:83–92. <https://doi.org/10.1016/j.cca.2017.04.026> PMID:[28465148](https://pubmed.ncbi.nlm.nih.gov/28465148/)
47. Vendrell JA, Vilquin P, Larrieux M, Van Goethem C, Solassol J. Benchmarking of amplicon-based next-generation sequencing panels combined with bioinformatics solutions for germline BRCA1 and BRCA2 alteration detection. *J Mol Diagn*. 2018; 20:754–64. <https://doi.org/10.1016/j.jmoldx.2018.06.003> PMID:[30055349](https://pubmed.ncbi.nlm.nih.gov/30055349/)
48. Shahid M, Choi TG, Nguyen MN, Matondo A, Jo YH, Yoo JY, Nguyen NN, Yun HR, Kim J, Akter S, Kang I, Ha J, Maeng CH, et al. An 8-gene signature for prediction of prognosis and chemoresponse in non-small cell lung cancer. *Oncotarget*. 2016; 7: 86561–72. <https://doi.org/10.18632/oncotarget.13357> PMID:[27863408](https://pubmed.ncbi.nlm.nih.gov/27863408/)
49. Duckworth C, Zhang L, Carroll SL, Ethier SP, Cheung HW. Overexpression of GAB2 in ovarian cancer cells promotes tumor growth and angiogenesis by upregulating chemokine expression. *Oncogene*. 2016; 35:4036–47. <https://doi.org/10.1038/onc.2015.472> PMID:[26657155](https://pubmed.ncbi.nlm.nih.gov/26657155/)
50. Wang Y, Sheng Q, Spillman MA, Behbakht K, Gu H. Gab2 regulates the migratory behaviors and E-cadherin expression via activation of the PI3K pathway in ovarian cancer cells. *Oncogene*. 2012; 31:2512–20. <https://doi.org/10.1038/onc.2011.435> PMID:[21996746](https://pubmed.ncbi.nlm.nih.gov/21996746/)
51. Linnerth-Petrik NM, Santry LA, Moorehead R, Jücker M, Wootton SK, Petrik J. Akt isoform specific effects in ovarian cancer progression. *Oncotarget*. 2016; 7:74820–33. <https://doi.org/10.18632/oncotarget.11204> PMID:[27533079](https://pubmed.ncbi.nlm.nih.gov/27533079/)
52. Cîrstea AE, Stepan AE, Zăvoi RE, Simionescu CE. EGFR immunoexpression in malignant serous and mucinous ovarian tumors. *Curr Health Sci J*. 2018; 44:129–34. <https://doi.org/10.12865/CHSJ.44.02.06> PMID:[30746159](https://pubmed.ncbi.nlm.nih.gov/30746159/)
53. Davies BR, Guan N, Logie A, Crafter C, Hanson L, Jacobs V, James N, Dudley P, Jacques K, Ladd B, D’Cruz CM, Zinda M, Lindemann J, et al. Tumors with AKT1E17K mutations are rational targets for single agent or combination therapy with AKT inhibitors. *Mol Cancer Ther*. 2015; 14:2441–51. <https://doi.org/10.1158/1535-7163.MCT-15-0230> PMID:[26351323](https://pubmed.ncbi.nlm.nih.gov/26351323/)
54. Bessièrè L, Todeschini AL, Auguste A, Sarnacki S, Flatters D, Legois B, Sultan C, Kalfa N, Galmiche L, Veitia RA. A hot-spot of in-frame duplications activates the oncoprotein AKT1 in juvenile granulosa cell tumors. *EBioMedicine*. 2015; 2:421–31. <https://doi.org/10.1016/j.ebiom.2015.03.002> PMID:[26137586](https://pubmed.ncbi.nlm.nih.gov/26137586/)
55. Grant DJ, Manichaikul A, Alberg AJ, Bandera EV, Barnholtz-Sloan J, Bondy M, Cote ML, Funkhouser E, Moorman PG, Peres LC, Peters ES, Schwartz AG, Terry PD, et al. Evaluation of vitamin D biosynthesis and pathway target genes reveals UGT2A1/2 and EGFR polymorphisms associated with epithelial ovarian cancer in African American Women. *Cancer Med*. 2019; 8:2503–13. <https://doi.org/10.1002/cam4.1996> PMID:[31001917](https://pubmed.ncbi.nlm.nih.gov/31001917/)
56. Ismail RS, Baldwin RL, Fang J, Browning D, Karlan BY, Gasson JC, Chang DD. Differential gene expression between normal and tumor-derived ovarian epithelial cells. *Cancer Res*. 2000; 60:6744–49. PMID:[11118061](https://pubmed.ncbi.nlm.nih.gov/11118061/)
57. Sherman-Baust CA, Weeraratna AT, Rangel LB, Pizer ES, Cho KR, Schwartz DR, Shock T, Morin PJ.

- Remodeling of the extracellular matrix through overexpression of collagen VI contributes to cisplatin resistance in ovarian cancer cells. *Cancer Cell*. 2003; 3:377–86.
[https://doi.org/10.1016/S1535-6108\(03\)00058-8](https://doi.org/10.1016/S1535-6108(03)00058-8)
PMID:12726863
58. Takano M, Kato M, Yoshikawa T, Sasaki N, Hirata J, Furuya K, Takahashi M, Yokota H, Kino N, Horie K, Goto T, Fujiwara K, Ishii K, et al. Clinical significance of UDP-glucuronosyltransferase 1A1*6 for toxicities of combination chemotherapy with irinotecan and cisplatin in gynecologic cancers: a prospective multi-institutional study. *Oncology*. 2009; 76:315–21.
<https://doi.org/10.1159/000209335> PMID:19299905
59. Cecchin E, Russo A, Corona G, Campagnutta E, Martella L, Boiocchi M, Toffoli G. UGT1A1*28 polymorphism in ovarian cancer patients. *Oncol Rep*. 2004; 12:457–62.
<https://doi.org/10.3892/or.12.2.457> PMID:15254716
60. Zhou Z, Lu Y, Song G, Wang Y, Chen J, Xiao C, Zhong L, Sun X, Peng Z, Wang X. In vitro study on influences of UGT1A8 gene polymorphisms on mycophenolate mofetil metabolism. *Exp Clin Transplant*. 2018; 16: 466–72.
<https://doi.org/10.6002/ect.2017.0017>
PMID:29025387
61. Pugazhenth S, Boras T, O'Connor D, Meintzer MK, Heidenreich KA, Reusch JE. Insulin-like growth factor I-mediated activation of the transcription factor cAMP response element-binding protein in PC12 cells. Involvement of p38 mitogen-activated protein kinase-mediated pathway. *J Biol Chem*. 1999; 274:2829–37.
<https://doi.org/10.1074/jbc.274.5.2829>
PMID:9915817
62. De Luca A, Maiello MR, D'Alessio A, Pergameno M, Normanno N. The RAS/RAF/MEK/ERK and the PI3K/AKT signalling pathways: role in cancer pathogenesis and implications for therapeutic approaches. *Expert Opin Ther Targets*. 2012 (Suppl 2); 16:S17–27.
<https://doi.org/10.1517/14728222.2011.639361>
PMID:22443084
63. Xie X, Liu X, Zhang Q, Yu J. Overexpression of collagen VI $\alpha 3$ in gastric cancer. *Oncol Lett*. 2014; 7:1537–43.
<https://doi.org/10.3892/ol.2014.1910>
PMID:24765172
64. Ao R, Guan L, Wang Y, Wang JN. Silencing of COL1A2, COL6A3, and THBS2 inhibits gastric cancer cell proliferation, migration, and invasion while promoting apoptosis through the PI3k-Akt signaling pathway. *J Cell Biochem*. 2018; 119:4420–34.
<https://doi.org/10.1002/jcb.26524>
PMID:29143985
65. Uddin M, Thiruvahindrapuram B, Walker S, Wang Z, Hu P, Lamoureux S, Wei J, MacDonald JR, Pellecchia G, Lu C, Lionel AC, Gazzellone MJ, McLaughlin JR, et al. A high-resolution copy-number variation resource for clinical and population genetics. *Genet Med*. 2015; 17:747–52.
<https://doi.org/10.1038/gim.2014.178>
PMID:25503493
66. Huang W, Sherman BT, Lempicki RA. Bioinformatics enrichment tools: paths toward the comprehensive functional analysis of large gene lists. *Nucleic Acids Res*. 2009; 37:1–13.
<https://doi.org/10.1093/nar/gkn923>
PMID:19033363
67. Huang W, Sherman BT, Lempicki RA. Systematic and integrative analysis of large gene lists using DAVID bioinformatics resources. *Nat Protoc*. 2009; 4:44–57.
<https://doi.org/10.1038/nprot.2008.211>
PMID:19131956
68. Mou HZ, Xu SH, Zhang YY. The establishment of human ovarian carcinoma cell line HO-8910 and its characteristics. *Zhonghua Fu Chan Ke Za Zhi*. 1994; 29:162–64, 191.
PMID:8082435
69. Liu Y, Han Y, Zhang H, Nie L, Jiang Z, Fa P, Gui Y, Cai Z. Synthetic miRNA-mowers targeting miR-183-96-182 cluster or miR-210 inhibit growth and migration and induce apoptosis in bladder cancer cells. *PLoS One*. 2012; 7:e52280.
<https://doi.org/10.1371/journal.pone.0052280>
PMID:23284967
70. Roider HG, Manke T, O'Keeffe S, Vingron M, Haas SA. PASTAA: identifying transcription factors associated with sets of co-regulated genes. *Bioinformatics*. 2009; 25:435–42.
<https://doi.org/10.1093/bioinformatics/btn627>
PMID:19073590
71. Oh HS, Moharita A, Potian JG, Whitehead IP, Livingston JC, Castro TA, Patel PS, Rameshwar P. Bone marrow stroma influences transforming growth factor-beta production in breast cancer cells to regulate c-myc activation of the preprotachykinin-I gene in breast cancer cells. *Cancer Res*. 2004; 64:6327–36.
<https://doi.org/10.1158/0008-5472.CAN-03-3122>
PMID:15342422